ARTICLE

Graphene Nanoribbons Obtained by Electrically Unwrapping Carbon Nanotubes

Kwanpyo Kim, Allen Sussman, and A. Zettl*

Department of Physics, University of California at Berkeley, Center of Integrated Nanomechanical Systems, University of California at Berkeley, Materials Sciences Division, Lawrence Berkeley National Laboratory, Berkeley, California 94720

ABSTRACT We describe a clean method of graphene nanoribbon (GNR) extraction from multiwall carbon nanotubes (MWNTs), performed in a high vacuum, nonchemical environment. Electrical current and nanomanipulation are used to unwrap a portion of the MWNT and thus produce a GNR of desired width and length. The unwrapping method allows GNRs to be concurrently characterized structurally *via* high-resolution transmission electron microscopy (TEM) and evaluated for electrical transport, including situations for which the GNR is severely mechanically flexed. High quality GNRs have exceptional current-carrying capacity, comparable to the exfoliated graphene.

KEYWORDS: graphene nanoribbon · carbon nanotube · *in situ* TEM

Graphene nanoribbons (GNRs) are attractive candidates for nanoelectronics, spintronics, and nanoelectromechanical systems (NEMS).[1−12] Lithographic and chemical methods have been used previously to produce GNRs from layered graphite or suitably prepared graphene.[1−3,6] Alternatively, GNRs have been produced from multiwall carbon nanotubes (MWNTs) using chemical oxidation, argon plasma etching, intercalation, or metal particle-assisted unzipping.[7−12] High-quality (typically arc-grown) MWNTs are attractive starting materials as they display excellent current carrying capacity indicative of low defect concentration.[13,14] Interestingly, nanoribbons derived from collapsed carbon nanotubes were reported already in 1995.[15] Employing MWNTs or single-wall nanotube (SWNTs) with narrow diameter distributions, unzipping approaches offer the possibility of large-scale production of narrow GNRs with well-controlled widths. Unfortunately, available unzipping methods have serious drawbacks related to surface contamination and introduction of structural defects, resulting in mechanical and electrical degradation.[7−12] Highly desirable would be a MWNT unwrapping method with no reliance on harsh chemical or other detrimental treatment, with the ability to preserve (or even enhance) the quality of the MWNT fabric. Electrical current-induced unwrapping of MWNTs for GNR production is an interesting approach to this requirement.

At very high electrical bias, MWNTs can display superplasticity,[16,17] or undergo structural failure through concentric wall-by-wall breakdown or blow-out with associated staircase-like current drops.[13,14,18,19] In vacuum, this breakdown is believed to be driven by resistive heating and thermal bond breaking (as opposed to oxidation, as might occur during blow-out in air[13]). Evidence for graphene flake production from MWNTs using high dc pulses has been recently reported.[20] We here apply the technique of current-induced electrical breakdown of MWNTs to produce GNRs. The key is to avoid the typical catastrophic wall blow-out, but instead promote controlled thermally induced unwrapping of the outer walls of the nanotube. Using *in situ* transmission electron microscopy (TEM), we also characterize GNRs structurally and electrically, including situations for which the GNR is severely mechanically flexed. GNRs derived from this method have high current-carrying capacity, which demonstrates that this is a promising technique for obtaining high quality GNRs from MWNTs.

RESULTS AND DISCUSSION

Figure 1 shows schematic drawings of the proposed fabrication process of extracting a GNR from a MWNT. Using a movable electrode, a MWNT is contacted and unwrapping of the outer walls is induced *via* an applied electrical current through the

*Address correspondence to azettl@berkeley.edu.

Received for review December 7, 2009 and accepted January 28, 2010.

Published online February 4, 2010. 10.1021/nn901782g

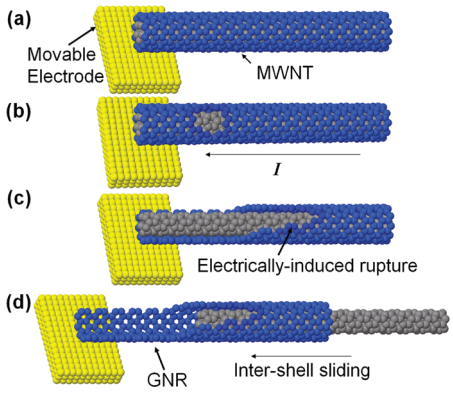

Figure 1. Schematic drawings of the proposed graphene nanoribbon (GNR) fabrication from a multiwall carbon nanotube (MWNT). In the schematic, a double-wall carbon nanotube (DWNT) is chosen for simplicity: (a) MWNT before the partial wall rupture; (b) electrical current induces rupture of the outer wall of a MWNT; (c) partial outer-wall rupture of a MWNT results in a precursor GNR which is under the MWNT inner core; (d) intershell sliding between the GNR and the inner core results in a suspended, electrically contacted GNR.

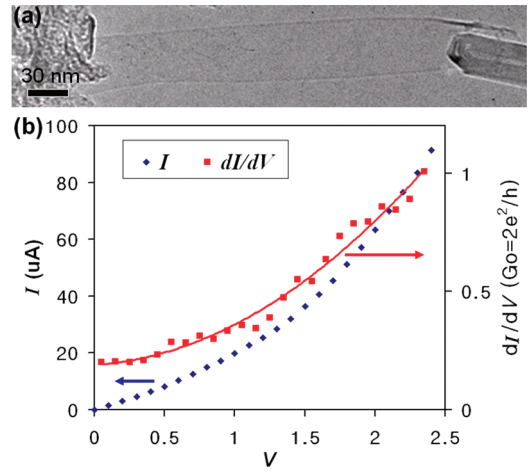

Figure 2. TEM images and electrical transport measurement of a GNR derived from a MWNT. (a) TEM image of a GNR derived from a MWNT *via* the electrical rupture and unwrapping method. The original MWNT from which the GNR is derived is shown on the right side; it continues to serve as a mechanical support and electrical contact for the GNR. (b) Electrical transport measurement of the same GNR. The blue diamond and red square dots (color online) are the electrical current and differential conductance at given voltages, respectively. The solid line is a guide to the eye for the differential conductance. At low voltages (<0.5 V), the response is linear. With higher bias, the conductance increases with increasing bias.

contact and tube. With proper voltage bias control, only part of the MWNT outer wall (upper portion in the schematic) is severed and, as shown in Figure 1c, a precursor GNR is created which clings to the remaining MWNT inner core. The GNR is then systematically removed from the MWNT *via* sliding between the GNR and the MWNT inner core, as shown in Figure 1d. The newly formed GNR can easily be completely removed from the MWNT, or, most importantly, the sliding process can be terminated when a desired amount of GNR has been slid off. This leaves a preselected length of GNR fully suspended in vacuum, with each end electrically and mechanically attached to a conducting electrode (the remaining portion of the MWNT serves as one electrode).

Figure 2a shows a TEM image of a GNR experimentally derived from a MWNT using the electrical-current-induced unwrapping technique. The GNR is fully suspended in vacuum, with each end electrically and mechanically attached to a conducting electrode. The original MWNT (30 nm diameter) from which the GNR is derived is located on the right side of the GNR. The length of the GNR is about 300 nm and the width, uniform along the ribbon axis, is 45 nm, suggesting about half (circumferentially) of the MWNT outermost shells were vaporized during the electrical unwrapping process. The proposed unwrapping of MWNTs is a very fast process and the intermediate steps of it were not observed in our TEM experiments due to spatial and temporal limitations. However, this is a very likely scenario and supporting evidence for this unwrapping of MWNTs is documented in Figure 5. Related modeling of the thermally induced nanotube wall-rupture mechanism is also discussed later in this article and the Supporting Information. The edge of the GNR in Figure 2a could not be resolved at the atomic scale, posing the possibility that this structure is a collapsed nanotube.

Considering that a collapsed nanotube is within the GNR family, we use the term GNR for this structure.[15] In Figure 2b, the two-terminal electrical transport for the same GNR is shown. The blue diamond and red square dots are, respectively, the electrical current and differential conductance at given bias voltages. At low bias voltages (<0.5 V), the response is mostly linear, while at higher voltages the conductance increases with increasing bias voltage, similar to the behavior observed in MWNT two-terminal electrical transport measurements.[18]

Graphene and GNRs have remarkable mechanical properties[6,21−23] which make them promising materials for NEMS and flexible devices. To exploit graphene and GNRs for electromechanical purposes, it is crucial to characterize electrical transport under mechanical deformation conditions, but there have been few studies on this subject. The conductance of graphene films has been observed to drop reversibly when the films are subjected to bending or stretching.[21] The GNR isolation and mounting configuration described here affords highly controlled reversible flexing and simultaneous electrical measurement of a single GNR. Figure 3 panels a−c show a series of TEM images acquired during a mechanical deformation of the GNR. Clearly, the GNR shows dramatic distortions as the MWNT electrode is moved to the left, closing the gap between the electrodes. As the degree of flexing is changed, concurrent two-terminal electrical transport measurements are performed. Figure 3d shows *I*−*V* curves for each deformation state (a−c) of the GNR. The main result is that

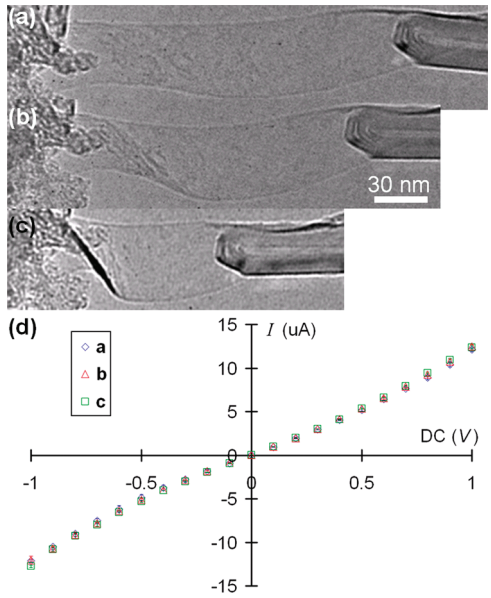

Figure 3. Flexing of a GNR and concurrent electrical measurement. (a−c) Sequential TEM images during the flexing process; (d) *I*−*V* curves for corresponding flexed states of the GNR in panels a−c. The two-terminal conductance stays the same even with the dramatic mechanical deformation of the GNR.

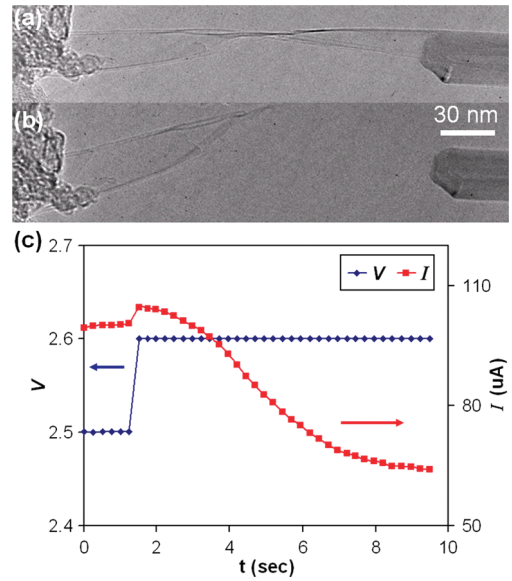

Figure 4. Electrical breakdown of a GNR. (a) TEM image of a GNR after partial electrical breakdown. The central part of the GNR has shrunk which implies diffusive electrical transport processes along the GNR. (b) TEM image of the GNR after total breakdown. (c) Voltage and current variation in time during the electrical breakdown. Stable two-dimensional maximum electrical current density is about 22 A/cm. The lack of a staircase-like current drop suggests that the GNR undergoes gradual, not quantized, breakdown.

the two-terminal resistance remains constant even with dramatic flexing of the GNR. This indicates that conductivity of GNRs (and presumably properly mounted graphene) can be maintained even under severe mechanical deformations such as high angle flexing. These results would also imply that rippling, which can occur on suspended graphene,[24] does not substantially modify the intrinsic electrical transport properties of graphene or its derivatives.

The ultimate current-carrying capacity of GNRs, and their failure mode under extreme bias conditions, is of great interest. We find that suspended GNRs can carry large currents without failure. For the specimen of Figure 2, a maximum two-dimensional current density of ~22 A/cm is obtained, comparable to that found for exfoliated graphene on a substrate.[25,26] Notably, the GNR is here suspended in vacuum, and thus the central portion is not well thermally anchored and presumably at elevated temperature. This suggests an even higher ultimate current limit is possible for thermally anchored GNRs.

Figure 4 shows the results of a suspended GNR intentionally driven to electrical failure. TEM images of the GNR and corresponding transport data are shown. As seen in Figure 4c, the GNR is stable and the current remains constant (~100 μA) for an applied bias of 2.5 V. As the bias is increased to 2.6 V, the current begins to drop and the middle part of the GNR diminishes in width (Figure 4a). With fixed bias, the current asymptotically approaches ~65 μA as shown in Figure 4c. During the GNR breakdown, no staircase-like current drops are observed, indicating no dramatic "quantized" geometrical configurations; the GNR width gradually and smoothly diminishes. As the electrical bias is increased to ~3 V, the GNR fails catastrophically at the central part and current drops to zero, as shown in Figure 4b. The breakdown mechanism of the GNR under high bias is likely due to carbon atom sublimation from the GNR edges due to high temperatures.[27,28] Related current-induced "shrinking" of carbon nanotubes has been reported.[29]

We now examine in more detail the electrically induced MWNT rupture and unwrapping mechanism that leads to GNR formation. The key is the asymmetric electrode contact at the tip of the MWNT. This side-contacting results in asymmetric electrical and thermal transport conditions near the tip of the MWNT. Most notably, this results in a sharp temperature difference between the noncontacted and contacted outer surfaces of the MWNT near its tip. The noncontact side of the MWNT tip achieves a higher temperature than the contact side, and this is where the unwrapping (ejection of carbon atoms) is initiated. The asymmetric breakdown process is documented in Figure 5. Figure 5 panels a−e show a series of TEM images for the asymmetric side-contact condition. At the bottom of the MWNT tip, amorphous carbon and MWNT composite serve as an electrode. As the bias on the MWNT is increased, the onset of MWNT shell breakdown occurs, as shown in Figures 5b,c. The noncontact side of the MWNT tip experiences faster electrical breakdown. Along with the breakdown, the inner core shells of

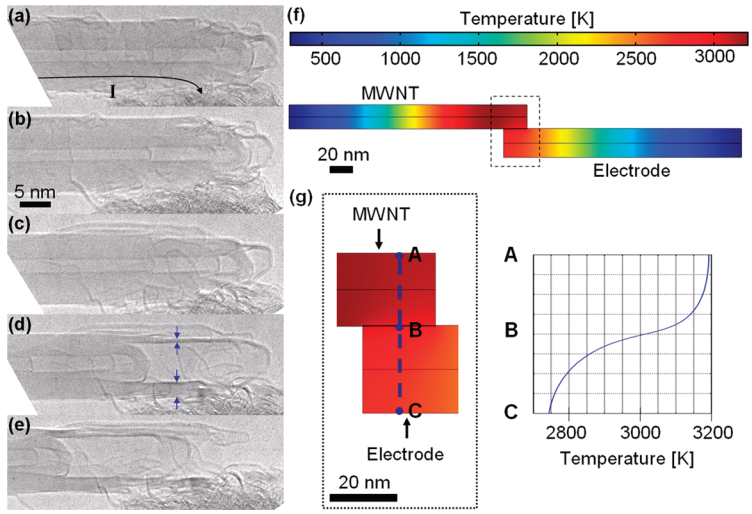

Figure 5. Asymmetric rupture of outer shells of a MWNT. (a−e) Sequential TEM images of an asymmetric rupture of MWNT outer shells. (a) Electrical current passes though the MWNT. At the bottom of the MWNT tip, MWNTs and amorphous carbon composite serve as an electrode. (b,c) MWNT walls start to undergo an electrical rupture. The noncontacted side of the MWNT tip ruptures first. (d) The inner core of MWNT slides to the left with respect to the outer shells. In the outer shells, it is clear that the contact side of the tip has more layers (eight layers) than the noncontact side (two layers). (e) The inner core of the MWNT slides farther with respect to the outer shells. Around the MWNT tip, a GNR-like structure appears. (f) Temperature profile of a MWNT and an electrode contacting the side of the tip from finite element analysis. Because of Joule heating, the area near the MWNT-electrode contact generally has a higher temperature than other parts of the system, reaching temperatures above 3000 K. (g) Zoomed-in image and temperature profile of the MWNT tip contact region. Temperature profile along line ABC shows that the noncontact side of the MWNT reaches higher temperatures than the contact side because the electrode acts as a heat sink.

the MWNT easily slide with respect to the outer shells, as shown in Figure 5d, due to thermal agitation. The contact side of the MWNT tip in Figure 5d has more intact layers (eight layers) than the noncontact side (two layers), as indicated by the arrows, which shows clearly that the wall breakdown occurs faster in the noncontact side. MWNT walls at the contact side, which do not have corresponding walls at the other side, readily evolve to low-curvature strips with edges—that is, GNRs. In Figure 5e, the inner core of the MWNT can be seen displaced left with respect to the outer shells. The GNR structures are now nearly isolated.

We carry out finite element analysis on a side-contact MWNT geometry to quantify the asymmetric temperature distribution at the MWNT tip. The detailed analysis procedure is presented in the Supporting Information. We model the MWNT in the high-bias limit as a single cylinder with uniform, isotropic conductivity.[13,14,19,29] Figure 5f shows the simulated temperature profile of a MWNT and an electrode contacting the side of the MWNT tip. Because of Joule heating, the area near the MWNT-electrode contact generally has a higher temperature than other parts of the system, reaching temperatures above 3000 K. A close look at the temperature profile of the MWNT tip shows that the noncontact side reaches higher temperatures than the contact side (Figure 5g). This results from the electrode serving as a heat sink. The width of the MWNT wall segment that is above the critical temperature for carbon sublimation (approximately 3200 K[30]), along with MWNT outer circumference, dictates the final GNR width.

METHODS

TEM Experiments. Experiments are carried out inside a JEOL 2010 transmission electron microscope (TEM) operated at 100 keV, employing a nanomanipulation platform (Nanofactory Instruments AB). We choose this low acceleration voltage to minimize electron beam damages to MWNTs and GNRs. Arc-grown MWNTs are attached to an aluminum wire using conductive epoxy and the wire is then mounted to the stationary side of the holder. An etched tungsten probe is mounted to the opposite mobile side of the holder. Although the bare tungsten probe can itself serve as the mobile electrode, typically this electrode is first coated with a bundle of MWNTs or amorphous carbon−MWNT composite which facilitates carbon−carbon contact between the mobile electrode and the MWNT to be unwrapped. The probe is moved such that the mobile electrode touches the tip of a MWNT on the wire, creating a carbon−MWNT contact. A stable electrical and mechanical contact at the junction is established by annealing with high current. The sliding process between MWNT core and shell/GNR is maintained at a rate of 1−10 nm/sec. A Keithley 2400 SourceMeter is used for electrical bias and current readout across the MWNT. Five nanotubes have been unwrapped using this electrical breakdown method.

Finite Element Analysis. We use COMSOL Multiphysics, a commercially available finite element modeler. For the details of simulation, please refer to the accompanying Supporting Information.

Acknowledgment. We thank B. Kessler and Z. Lee for helpful discussions. This research was supported in part by the Director, Office of Energy Research, Office of Basic Energy Science, Materials Sciences and Engineering Division, of the U.S. Depart-

ment of Energy under contract DE-AC02-05CH11231, which provided for fabrication and characterization of the graphene nanoribbons, and by the National Science Foundation within the Center of Integrated Nanomechanical Systems, under Grant EEC-0832819, which provided for theoretical analysis. K.K. acknowledges further support from a Samsung Scholarship.

Supporting Information Available: Details of finite element analysis. This material is available free of charge via the Internet at http://pubs.acs.org.

REFERENCES AND NOTES

1. Han, M. Y.; Özyilmaz, B.; Zhang, Y.; Kim, P. Energy Band-Gap Engineering of Graphene Nanoribbons. *Phys. Rev. Lett.* **2007**, *98*, 206805.
2. Chen, Z.; Lin, Y. M.; Rooks, M. J.; Avouris, P. Graphene Nano-Ribbon Electronics. *Phys. E* **2007**, *40*, 228–232.
3. Li, X.; Wang, X.; Zhang, L.; Lee, S.; Dai, H. Chemically Derived, Ultrasmooth Graphene Nanoribbon Semiconductors. *Science* **2008**, *319*, 1229–1232.
4. Son, Y. W.; Cohen, M. L.; Louie, S. G. Half-Metallic Graphene Nanoribbons. *Nature* **2006**, *444*, 347–349.
5. Son, Y. W.; Cohen, M. L.; Louie, S. G. Energy Gaps in Graphene Nanoribbons. *Phys. Rev. Lett.* **2006**, *97*, 216803.
6. Chen, C.; Rosenblatt, S.; Bolotin, K. I.; Kalb, W.; Kim, P.; Kymissis, I.; Stormer, H. L.; Heinz, T. F.; Hone, J. Performance of Monolayer Graphene Nanomechanical Resonators with Electrical Readout. *Nat. Nanotechnol.* **2009**, *4*, 861–867.
7. Kosynkin, D. V.; Higginbotham, A. L.; Sinitskii, A.; Lomeda, J. R.; Dimiev, A.; Price, B. K.; Tour, J. M. Longitudinal Unzipping of Carbon Nanotubes to Form Graphene Nanoribbons. *Nature* **2009**, *458*, 872–876.
8. Jiao, L.; Zhang, L.; Wang, X.; Diankov, G.; Dai, H. Narrow Graphene Nanoribbons from Carbon Nanotubes. *Nature* **2009**, *458*, 877–880.
9. Zhang, Z.; Sun, Z.; Yao, J.; Kosynkin, D. V.; Tour, J. M. Transforming Carbon Nanotube Devices into Nanoribbon Devices. *J. Am. Chem. Soc.* **2009**, *131*, 13460–13463.
10. Cano-Márquez, A. G.; Rodríguez-Macías, F. J.; Campos-Delgado, J.; Espinosa-González, C. G.; Tristán-López, F.; Ramírez-González, D.; Cullen, D. A.; Smith, D. J.; Terrones, M.; Veg-Cantú, Y. I. Ex-MWNTs: Graphene Sheets and Ribbons Produced by Lithium Intercalation and Exfoliation of Carbon Nanotubes. *Nano Lett.* **2009**, *9*, 1527–1533.
11. Elías, A. L. ; Botello-Méndez, A. R. ; Meneses-Rodríguez, D. ; González, V. J. ; Ramírez-González, D. ; Ci, L. ; Muñoz-Sandoval, E. ; Ajayan, P. M. ; Terrones, H. ; Terrones, M. Longitudinal Cutting of Pure and Doped Carbon Nanotubes To Form Graphitic Nanoribbons Using Metal Clusters as Nanoscalpels. *Nano Lett*. Published online August 19, 2009, http://dx.doi.org/10.1021/nl901631z.
12. Sinitskii, A.; Fursina, A. A.; Kosynkin, D. V.; Higginbotham, A. L.; Natelson, D.; Tour, J. M. Electronic Transport in Monolayer Graphene Nanoribbons Produced by Chemical Unzipping of Carbon Nanotubes. *Appl. Phys. Lett.* **2009**, *95*, 253108.
13. Collins, P. G.; Hersam, M.; Arnold, M.; Martel, R.; Avouris, P. Current Saturation and Electrical Breakdown in Multiwalled Carbon Nanotubes. *Phys. Rev. Lett.* **2001**, *86*, 3128–3131.
14. Collins, P. G.; Arnold, M. S.; Avouris, P. Engineering Carbon Nanotubes and Nanotube Circuits Using Electrical Breakdown. *Science* **2001**, *292*, 706–709.
15. Chopra, N. G.; Benedict, L. X.; Crespi, V. H.; Cohen, M. L.; Louie, S. G.; Zettl, A. Fully Collapsed Carbon Nanotubes. *Nature* **1995**, *377*, 135–138.
16. Huang, J. Y.; Chen, S.; Wang, Z. Q.; Kempa, K.; Wang, Y. M.; Jo, S. H.; Chen, G.; Dresselhaus, M. S.; Ren, Z. F. Superplastic Carbon Nanotubes. *Nature* **2006**, *439*, 281.
17. Huang, J. Y.; Chen, S.; Ren, Z. F.; Wang, Z.; Kempa, K.; Naughton, M. J.; Chen, G.; Dresselhaus, M. S. Enhanced Ductile Behavior of Tensile-Elongated Individual Double-Walled and Triple-Walled Carbon Nanotubes at High Temperatures. *Phys. Rev. Lett.* **2007**, *98*, 185501.
18. Huang, J. Y.; Chen, S.; Jo, S. H.; Wang, Z.; Han, D. X.; Chen, G.; Dresselhaus, M. S.; Ren, Z. F. Atomic-Scale Imaging of Wall-by-Wall Breakdown and Concurrent Transport Measurements in Multiwall Carbon Nanotubes. *Phys. Rev. Lett.* **2005**, *94*, 236802.
19. Yuzvinsky, T. D.; Mickelson, W.; Aloni, S.; Konsek, S. L.; Fennimore, A. M.; Begtrup, G. E.; Kis, A.; Regan, B. C.; Zettl, A. Imaging the Life Story of Nanotube Devices. *Appl. Phys. Lett.* **2005**, *87*, 083103.
20. Kim, W. S.; Moon, S. Y.; Bang, S. Y.; Choi, B. G.; Ham, H.; Sekino, T.; Shim, K. B. Fabrication of Graphene Layers from Multiwalled Carbon Nanotubes Using High dc Pulse. *Appl. Phys. Lett.* **2009**, *95*, 083103.
21. Kim, K. S.; Zhao, Y.; Jang, H.; Lee, S. Y.; Kim, J. M.; Kim, K. S.; Ahn, J. H.; Kim, P.; Choi, J. Y.; Hong, B. H. Large-Scale Pattern Growth of Graphene Films for Stretchable Transparent Electrodes. *Nature* **2009**, *457*, 706–710.
22. Bunch, J. S.; van der Zande, A. M.; Verbridge, S. S.; Frank, I. W.; Tanenbaum, D. M.; Parpia, J. M.; Craighead, H. G.; McEuen, P. L. Electromechanical Resonators from Graphene Sheets. *Science* **2007**, *315*, 490–493.
23. Lee, C.; Wei, X.; Kysar, J. W.; Hone, J. Measurement of the Elastic Properties and Intrinsic Strength of Monolayer Graphene. *Science* **2008**, *321*, 385–388.
24. Meyer, J. C.; Geim, A. K.; Katsnelson, M. I.; Novoselov, K. S.; Booth, T. J.; Roth, S. The Structure of Suspended Graphene Sheets. *Nature* **2007**, *446*, 60–63.
25. Girit, Ç. O.; Zettl, A. Soldering to a Single Atomic Layer. *Appl. Phys. Lett.* **2007**, *91*, 193512.
26. Moser, J.; Barreiro, A.; Bachtold, A. Current-Induced Cleaning of Graphene. *Appl. Phys. Lett.* **2007**, *91*, 163513.
27. Jia, X.; Hofmann, M.; Meunier, V.; Sumpter, B. G.; Campos-Delgado, J.; Romo-Herrera, J. M.; Son, H.; Hsieh, Y. P.; Reina, A.; Kong, J.; *et al*. Controlled Formation of Sharp Zigzag and Armchair Edges in Graphitic Nanoribbons. *Science* **2009**, *323*, 1701–1705.
28. Campos-Delgado, J.; Romo-Herrera, J. M.; Jia, X.; Cullen, D. A.; Muramatsu, H.; Kim, Y. A.; Hayashi, T.; Ren, Z.; Smith, D. J.; Okuno, Y.; *et al*. Bulk Production of a New Form of sp^2 Carbon: Crystalline Graphene Nanoribbons. *Nano Lett.* **2008**, *8*, 2773–2778.
29. Yuzvinsky, T. D.; Mickelson, W.; Aloni, S.; Begtrup, G. E.; Kis, A.; Zettl, A. Shrinking a Carbon Nanotube. *Nano Lett.* **2006**, *6*, 2718–2722.
30. Begtrup, G. E.; Ray, K. G.; Kessler, B. M.; Yuzvinsky, T. D.; Garcia, H.; Zettl, A. Probing Nanoscale Solids at Thermal Extremes. *Phys. Rev. Lett.* **2007**, *99*, 155901.